Article

Cell Metabolism

The Ca^{2+}-Dependent Release of the Mia40-Induced MICU1-MICU2 Dimer from MCU Regulates Mitochondrial Ca^{2+} Uptake

Graphical Abstract

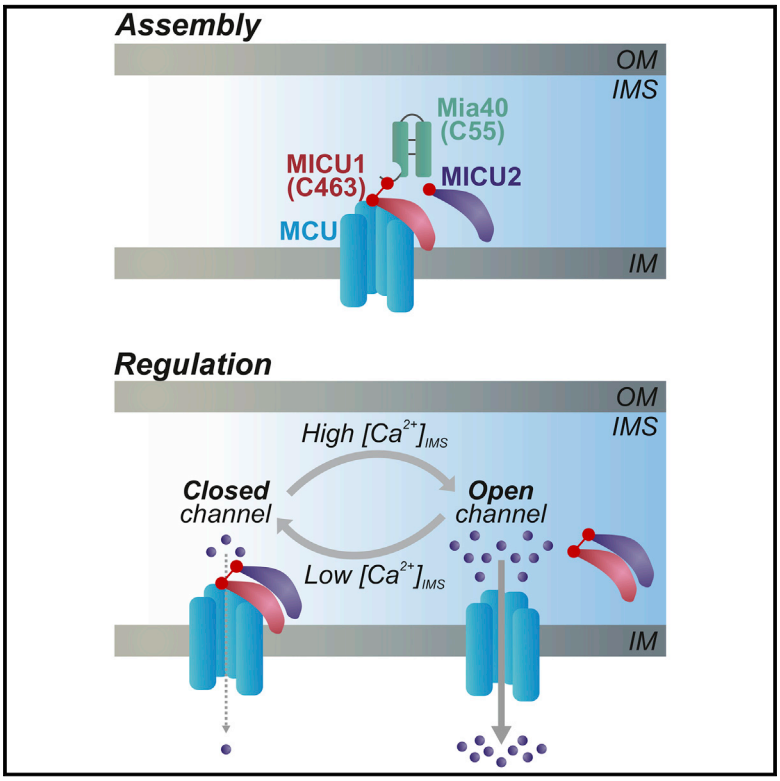

Authors

Carmelina Petrungaro, Katharina M. Zimmermann, Victoria Küttner, ..., Jörn Dengjel, Ivan Bogeski, Jan Riemer

Correspondence

jan.riemer@uni-koeln.de

In Brief

Petrungaro et al. characterize the interactome of the human mitochondrial oxidoreductase Mia40, among which is MICU1, the regulator of the mitochondrial Ca^{2+} uniporter (MCU). Mia40 primes MICU1 for heterodimerization with MICU2, and the dimer associates with MCU in a Ca^{2+}-dependent manner to control mitochondrial Ca^{2+} uptake.

Highlights

- Mia40 interactome links thiol redox to apoptosis, energy metabolism, Ca^{2+} signaling
- MCU serves as platform for disulfide-dependent MICU1-MICU2 dimerization by Mia40
- Absence of the disulfide that links MICU1 and MICU2 leads to increased Ca^{2+} uptake
- Ca^{2+} uptake is controlled by Ca^{2+}-dependent dissociation of the MICU dimer from MCU

Petrungaro et al., 2015, Cell Metabolism *22*, 721–733
October 6, 2015
http://dx.doi.org/10.1016/j.cmet.2015.08.019

Cell Metabolism
Article

The Ca^{2+}-Dependent Release of the Mia40-Induced MICU1-MICU2 Dimer from MCU Regulates Mitochondrial Ca^{2+} Uptake

Carmelina Petrungaro,[1,2] Katharina M. Zimmermann,[3] Victoria Küttner,[4] Manuel Fischer,[1] Jörn Dengjel,[4] Ivan Bogeski,[3] and Jan Riemer[1,2,*]
[1]Cellular Biochemistry, University of Kaiserslautern, Erwin-Schroedinger-Str. 13, 67663 Kaiserslautern, Germany
[2]Institute of Biochemistry, University of Cologne, Zuelpicher Str. 47, 50674 Cologne, Germany
[3]Department of Biophysics, CIPMM, School of Medicine, University of Saarland, 66421, Homburg, Germany
[4]Department of Dermatology, Medical Center, Freiburg Institute for Advanced Studies, BIOSS Centre for Biological Signaling Studies, ZBSA Center for Biological Systems Analysis, University of Freiburg, Habsburgerstr. 49, 79104 Freiburg, Germany
*Correspondence: jan.riemer@uni-koeln.de
http://dx.doi.org/10.1016/j.cmet.2015.08.019

SUMMARY

The essential oxidoreductase Mia40/CHCHD4 mediates disulfide bond formation and protein folding in the mitochondrial intermembrane space. Here, we investigated the interactome of Mia40 thereby revealing links between thiol-oxidation and apoptosis, energy metabolism, and Ca^{2+} signaling. Among the interaction partners of Mia40 is MICU1—the regulator of the mitochondrial Ca^{2+} uniporter (MCU), which transfers Ca^{2+} across the inner membrane. We examined the biogenesis of MICU1 and find that Mia40 introduces an intermolecular disulfide bond that links MICU1 and its inhibitory paralog MICU2 in a heterodimer. Absence of this disulfide bond results in increased receptor-induced mitochondrial Ca^{2+} uptake. In the presence of the disulfide bond, MICU1-MICU2 heterodimer binding to MCU is controlled by Ca^{2+} levels: the dimer associates with MCU at low levels of Ca^{2+} and dissociates upon high Ca^{2+} concentrations. Our findings support a model in which mitochondrial Ca^{2+} uptake is regulated by a Ca^{2+}-dependent remodeling of the uniporter complex.

INTRODUCTION

The mitochondrial intermembrane space (IMS) harbors a diverse set of proteins that fulfill important tasks (e.g., in mitochondrial protein import, detoxification of reactive oxygen species, and transport of metabolites). Moreover, the IMS takes a critical position in cellular signaling by relaying hydrogen peroxide signals, integrating cellular clues to initiate apoptosis, and supporting Ca^{2+} signaling (Herrmann and Riemer, 2010; Vögtle et al., 2012).

Import and folding of IMS proteins is mainly mediated by two pathways: some IMS proteins contain bipartite N-terminal targeting sequences (MTS) and employ the import machinery of the inner membrane (IM); however, import of most IMS proteins depends on their oxidative folding in the IMS (Chacinska et al., 2009; Herrmann and Riemer, 2010). Oxidation is performed by the oxidoreductase Mia40 (also CHCHD4), which contains a redox-active CPC motif (cysteine [C]; proline [P]; Figure 1A) (Banci et al., 2009; Kawano et al., 2009). The oxidized CPC motif can interact with precursor proteins that enter the IMS, leading to the formation of a mixed disulfide bond between conserved cysteines in the substrate and the CPC motif of Mia40 (Banci et al., 2009; Kawano et al., 2009; Milenkovic et al., 2009; Sideris et al., 2009). The precursor is eventually released in the oxidized form from Mia40, which is left behind in its reduced state (Bien et al., 2010; Terziyska et al., 2009). For another round of substrate oxidation, Mia40 is reoxidized by the sulfhydryl oxidase Erv1 (human homolog: augmenter of liver regeneration [ALR]) (Banci et al., 2011; Bien et al., 2010; Lionaki et al., 2010). Oxidation by Mia40 is possible despite the highly reducing environment of the IMS (with respect to the redox potential of the glutathione redox couple (Fischer et al., 2013; Kojer et al., 2012), because of low amounts of glutaredoxins in the IMS which protect protein thiols from reduction by glutathione.

Most so-far-known Mia40 substrates are small proteins (<15 kDa) that contain two α helices in each of which two cysteines are spaced by either three or nine residues (twin CX_3C and twin CX_9C proteins, respectively) (Gabriel et al., 2007; Herrmann and Riemer, 2010; Longen et al., 2009). Recently, in yeast, Mia40 substrates with different structures have been identified—the proteins copper chaperone for superoxide dismutase 1 (Ccs1) (Gross et al., 2011; Klöppel et al., 2011), Atp23 (Weckbecker et al., 2012), and Tim22 (Wrobel et al., 2013). For human Mia40, we know hardly any substrates, and we thus determined the interactome of human Mia40 and identified a set of Mia40 interaction partners, including the protein MICU1.

MICU1 is critical for mitochondrial Ca^{2+} signaling (Hajnóczky et al., 2003; Perocchi et al., 2010; Rizzuto et al., 2012). It is localized to the IM and forms a complex with the pore-forming mitochondrial Ca^{2+} uniporter (MCU) (Baughman et al., 2011; Chaudhuri et al., 2013; De Stefani et al., 2011), the MCU paralog MCUb (Raffaello et al., 2013), the regulatory subunit, MICU2 (Plovanich et al., 2013), and the essential MCU regulator (EMRE) (Sancak et al., 2013). MICU1 regulates MCU thereby facilitating a cooperative behavior during Ca^{2+} influx (Csordás et al., 2013; Kamer and Mootha, 2014). It maintains MCU closed at low Ca^{2+} levels

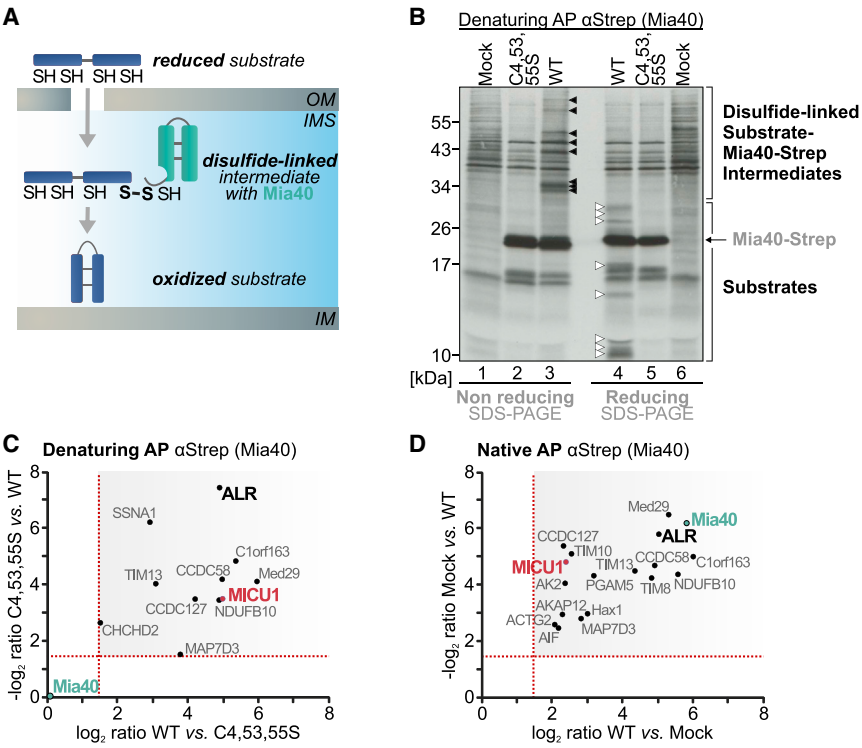

Figure 1. The Interactome of the Mitochondrial Oxidoreductase Mia40 Contains MICU1

(A) Mia40 can interact with and oxidize proteins in the mitochondrial IMS. Therefore, Mia40 relies on its redox-active cysteine motif (C53 and C55), which forms as part of the catalytic cycle a mixed-disulfide intermediate with the substrates.

(B) Pilot experiment to detect disulfide-linked Mia40-Strep interaction partners. Cells expressing either Mia40^{WT}-Strep, Mia40^{C4,53,55S}-Strep, or the empty vector (Mock) were pulse labeled for 4 hr, incubated with N-ethylmaleimide (NEM) to stabilize mixed disulfides, lysed under denaturing conditions, and incubated with strep-tactin beads. Bound proteins were eluted and analyzed by reducing and non-reducing SDS-PAGE. Black arrow heads: Substrate-Mia40 complexes. White arrow heads: Substrates that migrate alone after reduction of mixed disulfides between Mia40 and substrates.

(C) Interaction partners of Mia40^{WT}-Strep from denaturing affinity purification (AP). In this experiment only proteins interacting with Mia40 via a mixed disulfide bond are identified. Mia40^{WT}-Strep- and Mia40^{C4,53,55S}-Strep-expressing cells were grown in SILAC medium. Cells were treated with NEM, mixed and lysed under denaturing conditions. Mia40-Strep was enriched using strep-tactin beads and eluates were analyzed by mass spectrometry. The experiment was reproduced with inverted isotope labeling. Results from both experiments are plotted against each other. Proteins were counted as hits if at least two peptides per protein were enriched more than 2.8 fold.

(D) Interaction partners of Mia40^{WT}-Strep from native AP. In this experiment, one can identify both proteins interacting with Mia40 via a mixed disulfide bond and proteins that are non-covalently bound to Mia40. As (C) except that cells expressing Mia40^{WT}-Strep and cells harboring an empty vector (Mock) were assessed after native cell lysis.

and mediates opening of MCU at high Ca^{2+} concentrations to allow rapid Ca^{2+} transport across the IM. This induction of cooperative behavior of MCU by MICU1 requires two Ca^{2+}-binding EF-hands in MICU1 (Csordás et al., 2013; Kamer and Mootha, 2014). The role of MICU2 is less well defined: it can form heterodimers with MICU1 and modulates MCU activity likely in an inhibitory manner (Kamer and Mootha, 2014; Patron et al., 2014; Plovanich et al., 2013). The modulation thereby depends on the presence of MICU1 (Kamer and Mootha, 2014; Patron et al., 2014).

In this study we identify MICU1 as interaction partner of Mia40 and demonstrate that Mia40 mediates dimerization of MICU1 with MICU2. We show that at resting Ca^{2+} levels the MICU1-MICU2 heterodimer interacts with MCU. This interaction is lost at Ca^{2+} concentrations that stimulate mitochondrial Ca^{2+} uptake. A mutation of the disulfide-forming cysteine 463 in MICU1 results in the loss of the inhibitory component MICU2 from the complex which in turn leads to increased Ca^{2+} uptake. Based on our data, we propose that the Ca^{2+}-dependent association of the disulfide-linked MICU1 and MICU2 heterodimer with MCU enables the fine-tuned regulation of mitochondrial Ca^{2+} influx.

RESULTS

The Interactome of the Oxidoreductase Mia40

To identify the interactome of human Mia40, we combined precipitation of Mia40-substrate complexes with quantitative mass spectrometry. We constructed three stable inducible HEK293 cell lines to achieve the homogenous expression of C-terminally Strep-tagged Mia40 variants: one expressing wild-type Mia40 (Mia40^{WT}-Strep), one expressing a redox-inactive mutant of Mia40 (Mia40^{C4,53,55S}-Strep), and one that harbored an empty vector (Mock) (Figure S1A). We enriched Mia40-substrate complexes in a proof-of-concept experiment (Figure 1B). Precipitation of Mia40^{WT}-Strep but not Mia40^{C4,53,55S}-Strep or the Mock control yielded a number of bands that under non-reducing conditions migrated slower compared with Mia40-Strep alone (Figure 1B, black arrow heads). These bands disappeared when the samples were treated with a reductant. Instead, new bands appeared, all of them migrating faster than the bands observed in the non-reducing gel (Figure 1B, white arrow heads), indicating that the respective proteins had previously been connected to Mia40 by mixed disulfide bonds.

We next determined the identity of the interaction partners by quantitative mass spectrometry. Enriching Mia40-substrate complexes by denaturing immunoprecipitation (IP) led to the identification of eleven proteins (Figure 1C; Tables S1, S2, and S3). One of the hits was as expected ALR. We also identified the twin $CX_{3/9}C$ proteins Tim13 and CHCHD2/9, which are known interaction partners of Mia40 (Fischer et al., 2013). Moreover, we found eight novel Mia40 interaction partners: C1orf163, CCDC58, CCDC127, MAP7D3, Med29, NDUFB10, SSNA1, and MICU1.

Since Mia40 also contributes to import and folding of its substrates by non-covalent binding of hydrophobic residues in the substrate (Koch and Schmid, 2014; Weckbecker et al., 2012), we expanded our approach to Mia40 interaction partners that rely on the chaperone activity of Mia40. To this end, we compared Mia40^{WT}-Strep-containing samples to a Mock control after native cell lysis. With this approach, we found eighteen Mia40 interaction partners (Figure 1D; Tables S1 and S2). Among these enriched proteins were as expected all proteins that we identified in the denaturing precipitation. SSNA1 was only found enriched in one of the two biological replicates. In total, we identified additional eight interaction partners: ACTG2, adenylate kinase 2(AK2), AKAP12, apoptosis-inducing factor (AIF), HCLS1-associated protein X-1 (Hax1), phosphoglycerate mutase family member 5 (PGAM5), Tim8, and Tim10.

Taken together, we identified numerous targets of Mia40 including several uncharacterized open reading frames and proteins that potentially link the redox function of Mia40 to diverse IMS processes. Given the physiological importance of the interplay between redox and Ca^{2+} signaling and the nature of MICU1 as an unconventional Mia40 substrate, we focused on MICU1 to better understand how redox processes regulate mitochondrial Ca^{2+} homeostasis.

MICU1 Interacts with Cysteine 55 of Mia40 after Its Membrane-potential-dependent Import into the IMS

To confirm the interaction of MICU1 and Mia40, we utilized stable inducible cell lines expressing different Strep-tagged Mia40 variants (Figure S1A). We performed precipitations against the Strep tag after denaturing cell lysis. MICU1 did only coprecipitate with Mia40^{WT}-Strep and Mia40^{C53S}-Strep (Figure 2A), indicating that MICU1 interacts via a disulfide bond with cysteine 55 of Mia40. In contrast, the control protein LDH did not coprecipitate with Mia40.

We next performed the inverse experiment. To this end, we generated a stable inducible cell line that expressed MICU1 with a C-terminal HA epitope tag (MICU1-HA) (Figure S1B). Upon denaturing IP against the HA tag, we specifically coprecipitated endogenous Mia40 with MICU1-HA (Figure 2B). In a third approach, we then tested whether the endogenous proteins also interact with each other. Indeed, when endogenous MICU1 was immunoprecipitated, Mia40 was copurified (Figure 2C). Taken together, we confirmed MICU1 as interaction partner of Mia40.

Unlike most other Mia40 interaction partners, which rely on Mia40 for mitochondrial import, MICU1 contains a predicted MTS of 33 amino acid residues (Figure 2D). To investigate the import of endogenous MICU1 and the processing of its MTS, we performed pulse-chase assays and analyzed precipitated MICU1 on reducing SDS-PAGE (Figure 2D). Endogenous MICU1 migrated as a double band at around 55 kDa directly after pulse labeling. The slower migrating band likely represented the MICU1 precursor, as it was also observed when MICU1 import was prevented by depleting the mitochondrial membrane potential. During the chase time, MICU1 became further processed to a third band that migrated at around 45 kDa. The overall processing proceeded very slowly compared to the processing of the IMS protein Smac that, like MICU1, contains an MTS but becomes processed almost completely already during the pulse time (Figure S2A).

When during its membrane-potential-dependent import does MICU1 interact with Mia40? To answer this question we followed the disulfide-linked MICU1-Mia40 complex over time by pulse-chase analyses (Figure 2E). To this end, we first precipitated Mia40 from cells expressing MICU1-HA and then re-precipitated in a second step the HA-tagged MICU1, which was disulfide-linked to Mia40. Mia40 and MICU1 interacted strongest between 20 and 60 min of chase time (Figure 2E), suggesting a post-import interaction of both proteins.

As a consequence of the membrane-potential-dependent MICU1 import, the interaction between Mia40 and MICU1 should also become membrane potential dependent. Indeed, the mixed disulfide between MICU1 and Mia40 could only be observed in the presence of the mitochondrial membrane potential (Figures 2F and 2G). Conversely, the interaction between Mia40 and twin CX_nC substrate proteins was unaffected by the membrane potential (Figures 2F and 2G). Taken together, we find that MICU1 becomes imported in a membrane-potential-dependent and Mia40-independent manner (Figure S3). This membrane potential dependency also allowed to generally distinguish between co- and post-import interactions and suggested that MICU1 is not the only substrate that undergoes a post-import interaction with Mia40 (Figure S3A). After import, MICU1 forms a disulfide-linked complex with Mia40 (Figure 2H).

The Second Processing Step of MICU1 Takes Place Concomitantly to MICU1-MICU2 Dimerization by Mia40

The interaction between Mia40 and MICU1 is consistent with the recent report that MICU1 forms a disulfide-linked heterodimer with MICU2 (Patron et al., 2014). To address the role of Mia40 for the disulfide bond formation, we first explored the oxidation kinetics of MICU1 and MICU2 (Figure 3A; for processing of MICU2, see Figures S2B and S2C). We thereby found that both endogenous MICU1 and MICU2 mature within 30–90 min into complexes with apparent masses of approximately 96 kDa. Upon reduction, these complexes disappeared, indicating that they were linked by disulfide bonds. The 96 kDa complexes appeared to undergo dynamic changes that we attribute to processing of mainly MICU1 but also MICU2 (compare with processing kinetics in Figures 2D and S2A). In the absence of the membrane potential, this disulfide-linked dimer was not formed (Figure 3B), in line with the absence of Mia40-MICU1 complexes under these conditions (Figure 2F). Further analyses of MICU1 and MICU2 oligomerization revealed that upon MICU1 depletion, MICU2 failed to form heterodimers but was still processed to its mature form (Figure 3C). Conversely, MICU1 formed slower migrating homodimers upon MICU2 depletion (Figures 3D, S3H, and S3I) (Patron et al., 2014). This homodimerization proceeded slower than the heterodimerization between MICU1 and MICU2. Like for MICU2, all processing steps of MICU1 still occurred, indicating that heterodimerization is not required for processing, even though dimerization precedes the second processing step of MICU1 in the control situation (Figure S2D). When we correlated the dimerization kinetics of MICU1 with the kinetics of the Mia40-MICU1 interaction, we found that—as expected for an oxidoreductase and its substrate—the Mia40-MICU1 interaction preceded disulfide-dependent MICU1 dimerization (Figure 3E).

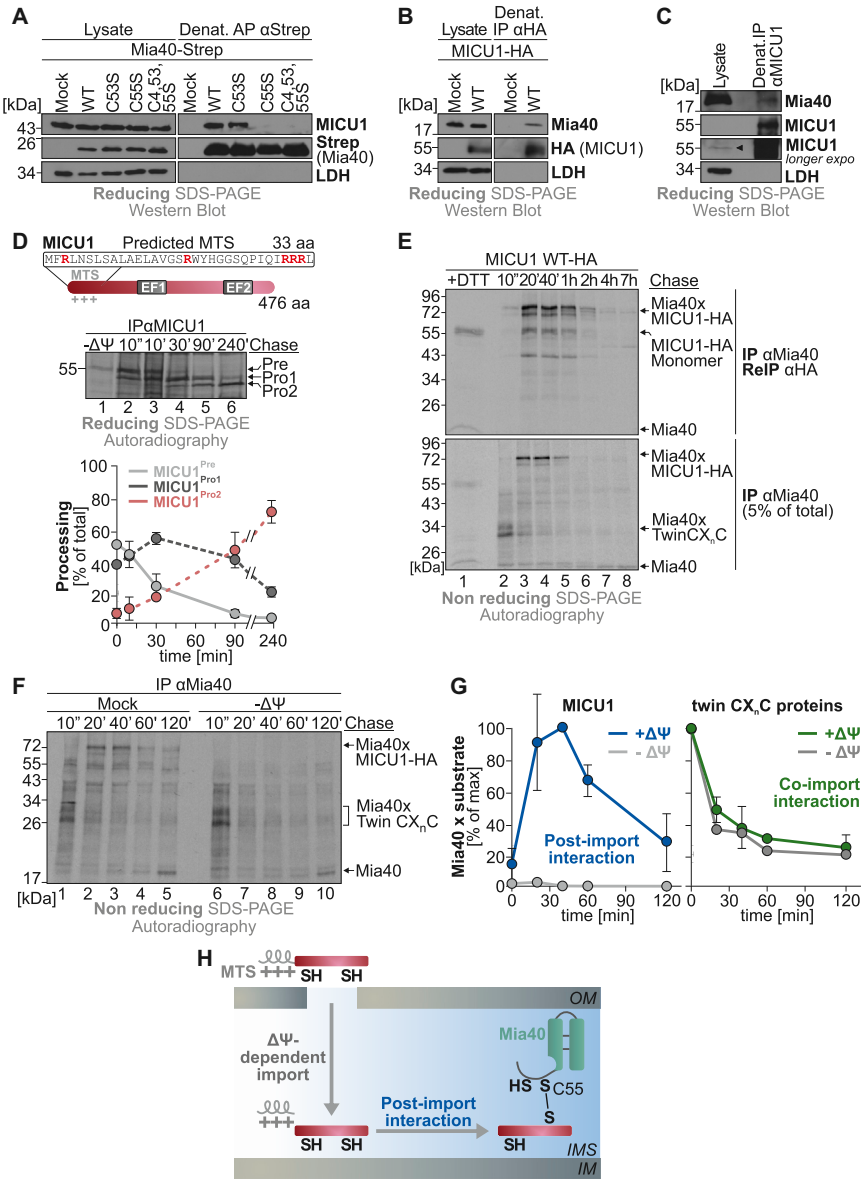

Figure 2. Interaction between MICU1 and Mia40 Takes Place after IMS Import of MICU1

(A) AP of Mia40-Strep variants and test for MICU1 interaction. Cells expressing different Mia40-Strep variants were treated with NEM and lysed under denaturing conditions, and Mia40-Strep variants were precipitated using strep-tactin beads. Immunoblot analyses were performed against MICU1, Strep, and as control LDH.

(B) Denaturing IP of MICU1-HA to test for interaction with Mia40. As (A) except that MICU1-HA was immunoprecipitated from cells expressing MICU1-HA or an empty vector (Mock). Immunoblot analyses were performed against HA, Mia40, and as control LDH.

(C) Test for interaction of endogenous Mia40 and endogenous MICU1. As (A) except that denaturing IP was performed against MICU1 in HEK293 cells. Eluates were analyzed by immunoblot against Mia40, MICU1, and LDH on reducing SDS-PAGE.

(D) Maturation of endogenous MICU1 is comparatively slow and involves multiple processing steps. Top: Domain layout of MICU1. It contains a predicted mitochondrial presequence (predicted by MitoProt2, TargetP) and two EF hands. Middle: Pulse-chase experiment (10 min pulse, indicated chase times) and subsequent IP against MICU1. Eluates were analyzed by reducing SDS-PAGE and autoradiography. As control the mitochondrial membrane potential was depleted by incubation with CCCP and valinomycin during the pulse and chase periods ($-\Delta\Psi$). Pre: precursor; Pro, Pro1, and Pro2: processed forms. Bottom: Quantifications. The intensities of the precursor and processed forms were analyzed with ImageJ. Error bars represent SD.

(E) The interaction of Mia40 with MICU1^{WT}-HA is delayed compared to its interaction with twin CX$_n$C substrates. Cells were pulse labeled for 10 min with [^{35}S]-methionine and chased with cold methionine for the indicated times. Cells were treated with NEM and lysed, and lysates analyzed by IP against Mia40. After the first IP against endogenous Mia40 (lower blot), the resulting eluate was analyzed by a second IP (ReIP) against HA (upper blot). Eluates were analyzed by non-reducing SDS-PAGE and autoradiography.

(F) The Mia40-MICU1^{WT}-HA interaction depends on the mitochondrial membrane potential. Experiment was performed as described in (E).To deplete the mitochondrial membrane potential, cells were incubated with CCCP and valinomycin during the pulse and chase periods ($-\Delta\Psi$). Cells were analyzed by IP against Mia40. Eluates were analyzed by non-reducing SDS-PAGE and autoradiography. The intensities of the Mia40-MICU1^{WT}-HA complex and Mia40-twin CX$_n$C protein complexes at different times were analyzed with ImageJ.

(G) Kinetics of Mia40-substrate interactions for co- and post-import interactions differ strongly. Quantification of (F). Error bars represent SD.

(H) Model for the membrane-potential-dependent interaction of Mia40 and MICU1.

In order to facilitate dimer formation, Mia40 has to interact with one of the cysteines of MICU1. MICU1 contains seven cysteine residues of which only cysteine 463 is conserved (Figure 3F). This cysteine has been reported to be involved in disulfide bond formation with MICU2 (Patron et al., 2014) and would thus also be expected to interact with Mia40. To test this, we generated MICU1 variants that each lack one of the seven cysteines (confirmation of mitochondrial localization; Figure S1B). When we analyzed these proteins on non-reducing SDS-PAGE, we could confirm that all MICU1 mutants formed the disulfide-linked MICU1 dimer except for MICU1^{C463A}-HA (Figures 3G, S3J, and S3K). This was not due to a mislocalization of this variant (Figures S1B and S2E). We next tested the interaction between MICU1^{C463A}-HA and Mia40 and showed that Mia40 co-precipitates with MICU1^{WT}-HA but not with MICU1^{C463A}-HA (Figure 3H).

Interestingly, in our experiments we only found MICU1 but not MICU2 to interact with Mia40 (Figure 3I), even though MICU1 and MICU2 share high structural and sequence similarity. Analysis of the amino acid sequence around cysteine 463 in

MICU1 revealed that cysteine 463 is present in an α helix and is flanked by hydrophobic residues that line the same face of the helix (Figure 3J). This motif is also found in the so-called IMS-targeting signal, which has been described to serve as recognition sequence of twin CX_nC-type Mia40 substrates (Koch and Schmid, 2014; Milenkovic et al., 2009; Sideris et al., 2009). MICU2 does not contain such a signal (Figure 3J), which explains why Mia40 specifically interacts with MICU1 but not MICU2.

Taken together, we find that MICU1 and MICU2 maturation includes an initial processing of MICU1 and MICU2 after membrane-potential-mediated mitochondrial import. Then, Mia40 forms a disulfide bond specifically with MICU1 but not MICU2, likely by recognizing a hydrophobic motif around cysteine 463. This interaction primes MICU1 for heterodimerization with MICU2. During or after dimerization MICU1 is processed a second time (Figure 3K).

Disulfide Bond Formation between MICU1 and MICU2 Takes Place on MCU

We next tested whether disulfide-dependent dimerization was critical for MCU-MICU1 complex formation. To this end, we constructed cell lines that stably coexpress MCU-FLAG and MICU1-HA variants (Figure S1C). Using these cell lines, we performed native IP experiments (using n-Dodecyl β-D-maltoside as mild solubilizing detergent) in which we precipitated either MICU1-HA or MCU-FLAG, respectively (Figures 4A and 4B). We thereby observed that $MICU1^{WT}$-HA and $MICU1^{C463A}$-HA both interacted with MCU-FLAG (Figure 4A). In line with this physical interaction of MCU with both MICU1 variants, we also observed a stabilization of especially $MICU1^{C463A}$-HA upon coexpression of MCU-FLAG (Figure 4C). The half-life of $MICU1^{C463A}$-HA was extended from 1 hr to 2.5 hr (Figures 4C). Also, the half-life of $MICU1^{WT}$ appeared to increase upon coexpression of MCU, although only to a minor extent. This indicates that the stoichiometry of MCU and MICU1 influences the stability of MICU1. Conversely, MCU has a longer half-life compared to MICU1 (Figure S4). The shorter half-life of $MICU1^{C463A}$-HA compared to $MICU1^{WT}$-HA indicates that the disulfide bond in the MICU dimer is structural, which is also supported by its high stability toward the reductant DTT (Figure S3L).

Because $MICU1^{C463A}$-HA also interacts with MCU-FLAG, it can be concluded that disulfide bond formation is not essential for the interaction between MICU1 and MCU. We therefore next analyzed whether $MICU1^{WT}$-HA also interacts with MCU-FLAG as monomer prior to its dimerization. To this end, we performed a pulse-chase experiment and isolated MCU-FLAG after different chase times by native IP. A subsequent denaturing re-IP against MICU1-HA showed that both $MICU1^{WT}$ and $MICU1^{C463A}$-HA interacted immediately after the pulse period with MCU-FLAG (Figure 4D) and became fully processed while being associated with MCU-FLAG. Taken together, our model for the assembly of the uniplex includes membrane-potential-dependent import of MICU1, MICU2, and MCU (Figures 2D, S2B, and S4A) followed by interaction of the MICU1 monomer with MCU (Figure 4D). Then, Mia40 primes MICU1 for heterodimerization with MICU2, which subsequently takes place on MCU (Figure 4E).

Preventing Disulfide-Dependent Heterodimerization between MICU1 and MICU2 Influences MCU Activity

MICU1 dimers and monomers are both parts of the mitochondrial uniplex (Figure 4), and we wondered how this influences mitochondrial Ca^{2+} uptake (for establishment of our Ca^{2+} measurements and comparison with previously published results, see Figure S5). We first examined the role of MICU1 cysteine 463 on mitochondrial Ca^{2+} uptake. To this end, we utilized mitochondrial targeted D3cpv and TN-XL as sensors to cover a wide range of matrix Ca^{2+} concentrations and transfected them in cells coexpressing MCU-FLAG with either $MICU1^{WT}$-HA or $MICU1^{C463A}$-HA (Figures 5A and 5B). Coexpression of $MICU1^{C463A}$ with MCU caused no significant changes in the basal $[Ca^{2+}]_{mito}$ when compared to $MICU1^{WT}$+MCU. However, ATP-induced Ca^{2+} uptake in $MICU1^{C463A}$+MCU cells was significantly increased and prolonged compared to $MICU1^{WT}$+MCU cells (Figures 5A and 5B).

MICU1 exists in a heterodimer with MICU2, and it has been proposed that MICU2 exhibits an inhibitory influence on Ca^{2+} uptake (Patron et al., 2014). We could confirm this finding (Figure S5I) and also found that when coexpressing MICU2 with MCU and $MICU1^{C463A}$, Ca^{2+} uptake was still significantly elevated 50 s after ATP addition compared to cells expressing $MICU1^{WT}$+MCU+MICU2 (Figure 5C). Mitochondrial Ca^{2+} uptake is controlled by Ca^{2+} levels in the IMS that equal cytosolic Ca^{2+} concentrations. Hence, we also tested if $MICU1^{C463A}$ affected cytosolic Ca^{2+} dynamics. Our results indicate no overt differences between MCU, MICU2, and either $MICU1^{WT}$ or $MICU1^{C463A}$ expression (Figures S5J and S5K).

In summary, these findings strongly support a critical role of MICU1 cysteine 463 and the disulfide-linked heterodimer for the regulation of mitochondrial Ca^{2+} uniplex activity. It was previously shown that MICU1 links MICU2 to the uniplex (Kamer and Mootha, 2014). It is therefore tempting to speculate that in the absence of the disulfide bond, MICU2 is hampered in exerting its function on the uniplex, while $MICU1^{C463A}$ might still fulfill the role of MICU1 in the uniplex.

Ca^{2+} Levels Determine the Amounts of MICU1-MICU2-Dimer in Complex with MCU

How can the regulation of MCU by the MICU heterodimer be explained on a molecular level? On the one hand, the disulfide bond might be reduced in the presence of Ca^{2+}. Due to the high stability of the disulfide (Figure S3L), this option appears unlikely, and we could show that heterodimerization is unaffected in the presence of different amounts of Ca^{2+} (Figure S3M). Alternatively, different Ca^{2+} levels might lead to structural changes in MICU1 and MICU2 and thus affect the binding of the heterodimer to MCU. To test this hypothesis, we analyzed the amounts of MICU1-MICU2 that were bound to MCU in dependence of Ca^{2+} (Figure 6A). We performed native IP against either MCU-FLAG or MICU1-HA in the presence or absence of Ca^{2+} and analyzed the levels of coprecipitated MICU1 or MCU, respectively (Figures 6B and 6C). Interestingly, MICU1-HA and MCU-FLAG interacted only in the absence but not in the presence of Ca^{2+} (Figures 6B and 6C). The Ca^{2+}-dependent dissociation of the MICU1-MCU complex did not depend on MICU2 since also monomeric $MICU1^{C463A}$-HA was not in a complex with MCU when the cells were lysed in the presence of Ca^{2+}

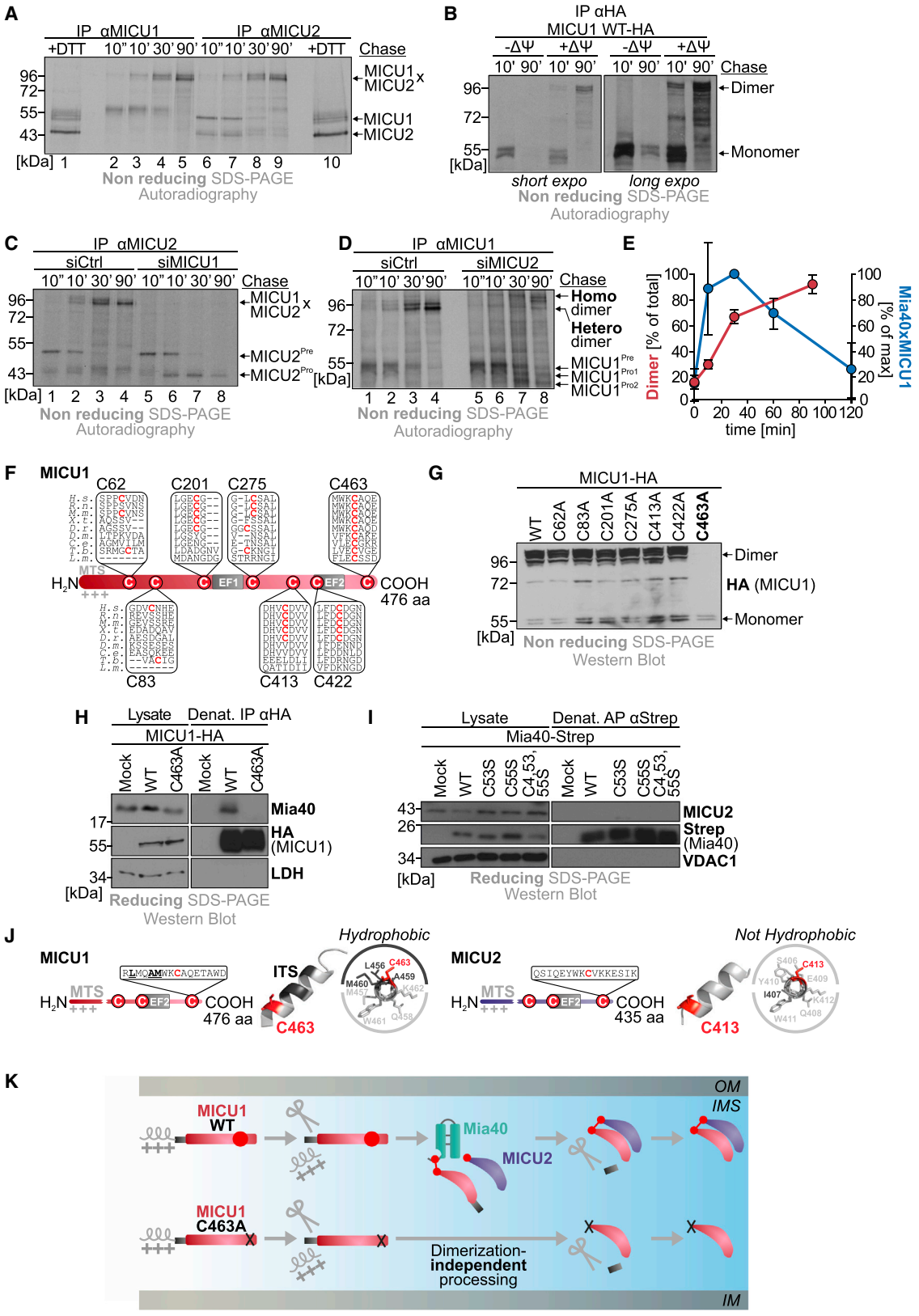

(legend on next page)

(Figure 6D). Next, we repeated the native IP against MCU-FLAG using a cell line that only expresses MCU-FLAG. In this cell line, the endogenous stoichiometry of MICU1 and MICU2 is preserved. Consistently, the amounts of endogenous MICU1-MICU2 dimer that coprecipitated with MCU-FLAG decreased at high Ca^{2+} concentrations (Figure 6E). MICU1 coprecipitated mainly in its monomeric form (likely representing an assembly intermediate), while MICU2 did not coprecipitate at all (Figure 6E).

To put these findings into a physiological context, we next correlated the Ca^{2+} concentrations that activate MCU-dependent Ca^{2+} uptake with those that lead to a release of the MICU-dimer from MCU (Figures 6F and 6G). To this end, we first semi-permeabilized cells expressing MCU, MICU2, and MICU1 and measured Ca^{2+} uptake induced by increasing external Ca^{2+} levels. At concentrations between 1 and 3 μM, the rate of mitochondrial Ca^{2+} uptake was highest (Figure 6F), which is in line with previously published results (Csordás et al., 2013). If MCU activation would require the dissociation of the MICU dimer, a concentration in the very low μM range should be sufficient to release MICU1 from MCU. To test this, we repeated the experiment shown in Figure 6B with different Ca^{2+} concentrations. Indeed, at 0.7 to 2 μM Ca^{2+}, the $MICU1^{WT}$-HA dimer showed reduced binding to MCU-FLAG (Figure 6G, upper blot). This dynamic behavior was dependent on the sensing of Ca^{2+} by the EF hands in MICU1 because a MICU1 mutant that lacked the Ca^{2+} binding motifs (ΔEF) did not respond to elevated Ca^{2+} levels (Figure 6G, lower blot). We confirmed this behavior also for endogenous MICU1 and MICU2 (Figure 6H). Noteworthy, Ca^{2+} had to be applied during cell lysis and not to the already lysed cells to observe this effect. Isolating the complex without Ca^{2+} and incubating it subsequently with Ca^{2+} did not result in a release of the MICU1 dimer from MCU-Flag (Figure S6). Taken together, our data support that the composition of the mitochondrial uniplex changes with differences in the local Ca^{2+} levels. At high concentrations of Ca^{2+} in the IMS, the MICU1-MICU2 dimer is released from the uniplex, while at resting conditions the dimer binds to MCU. Based on our Ca^{2+} measurements, we propose that these composition changes regulate uniplex activity (Figure 6I).

DISCUSSION

The Interactome of Mia40 Links Redox Homeostasis to a Variety of Mitochondrial Pathways

Here we identified interaction partners of Mia40 in human cells and thereby linked mitochondrial disulfide bond formation to a variety of mitochondrial functions, including Ca^{2+} signaling, apoptosis, and energy metabolism.

Many Mia40 interaction partners had already previously been localized to the IMS (Tables S1 and S2). All of them, except AIF, MICU1, and PGAM5, lack presequence-like MTS and are presumably imported into the IMS by the Mia40 pathway. AIF has also been shown to support import of Mia40 (Hangen et al., 2015). Consistently, most identified Mia40 interaction partners also contain conserved cysteines, and some even contain typical Mia40 recognition sites (Table S2). While most so-far-investigated Mia40 substrates are small proteins with a simple helix-loop-helix structure, some of the Mia40 interaction partners contain multiple conserved cysteines and multidomain structures (e.g., C1orf163 with 13 cysteines or MAP7D3 with a mass of ca 90 kDa and 5 cysteines). Thus, these proteins might in the future allow the detailed biophysical analyses of folding

Figure 3. Maturation of MICU1 Involves Multiple Processing Steps, Interaction with Mia40 and Subsequent Disulfide-Dependent Heterodimerization with MICU2

(A) MICU1 and MICU2 form heterodimers. Cells were pulse labeled for 10 min with [^{35}S]-methionine and chased with cold methionine for the indicated times. Cells were treated with NEM and lysed, and lysates were analyzed by IP against MICU1 or MICU2, respectively. Eluates were analyzed by non-reducing SDS-PAGE and autoradiography. +DTT: The 90′ chase sample was obtained twice and once treated with dithiothreitol (DTT) to reduce disulfide bonds.

(B) Disulfide-dependent dimerization of MICU1 depends on the mitochondrial membrane potential. Experiment was performed as described in (A) except that the membrane potential was depleted in two samples ($-\Delta\Psi$). Eluates of the IP against $MICU1^{WT}$-HA were analyzed by non-reducing SDS-PAGE and autoradiography.

(C) MICU1 depletion prevents dimerization of MICU2 but not MICU2 processing. HeLa cells were treated for 72 hr with control siRNA (siCtrl) or siRNA directed against MICU1. Then, dimerization kinetics of MICU2 was analyzed as described in (A). IP was performed against MICU2.

(D) MICU2 depletion leads to the formation of MICU1 homodimers and does not prevent the second processing step in MICU1. HeLa cells were treated for 48 hr with control siRNA (siCtrl) or siRNA directed against MICU2. Then, dimerization kinetics of MICU1 was analyzed as described in (A). IP was performed against MICU1.

(E) Mia40-MICU1 interaction precedes MICU1-MICU2 dimer formation. The MICU1 dimer formation in (A) was quantified with ImageJ. As a comparison, the quantification of the Mia40-$MICU1^{WT}$-HA interaction from Figure 2G was included. Error bars represent SD.

(F) Domain layout of human MICU1. MICU1 contains a mitochondrial targeting sequence (MTS), two EF hands, and seven cysteines, of which cysteine 463 is conserved.

(G) Mutational analysis of human MICU1 cysteines reveals cysteine 463 to be involved in MICU dimerization. Cells expressing single cysteine mutants of MICU1-HA were lysed after NEM treatment and analyzed by non-reducing SDS-PAGE and immunoblot against the HA tag.

(H) Mia40 and MICU1 interact via cysteine 463 in MICU1. Cells expressing $MICU1^{WT}$-HA, $MICU1^{C463A}$-HA, or an empty vector (Mock) were treated with NEM and lysed under denaturing conditions. IP against the HA tag was performed, and the eluates were analyzed by immunoblot against the HA tag, Mia40, and as control LDH.

(I) MICU2 does not interact with Mia40. Experiment was performed as described in Figure 2A. Immunoblot analyses were performed against MICU2, Strep, and as control VDAC1.

(J) MICU1 but not MICU2 contains a potential Mia40 interaction site. C463 of MICU1 (PDB: 4NSC) is surrounded by hydrophobic amino acids forming an IMS-targeting sequence that is crucial for the interaction with Mia40. The structure of MICU2 was modeled based on the structure of MICU1 using SWISS-MODEL. C413 of MICU2 is not surrounded by hydrophobic residues. This likely prevents the interaction with Mia40.

(K) Model for MICU1 maturation. MICU1 is processed directly after translocation into mitochondria. Then, Mia40 interacts with MICU1 to prime it for heterodimerization with MICU2. After or during dimerization, a second processing step takes place in MICU1. Notably, dimerization is not a prerequisite for this second processing step.

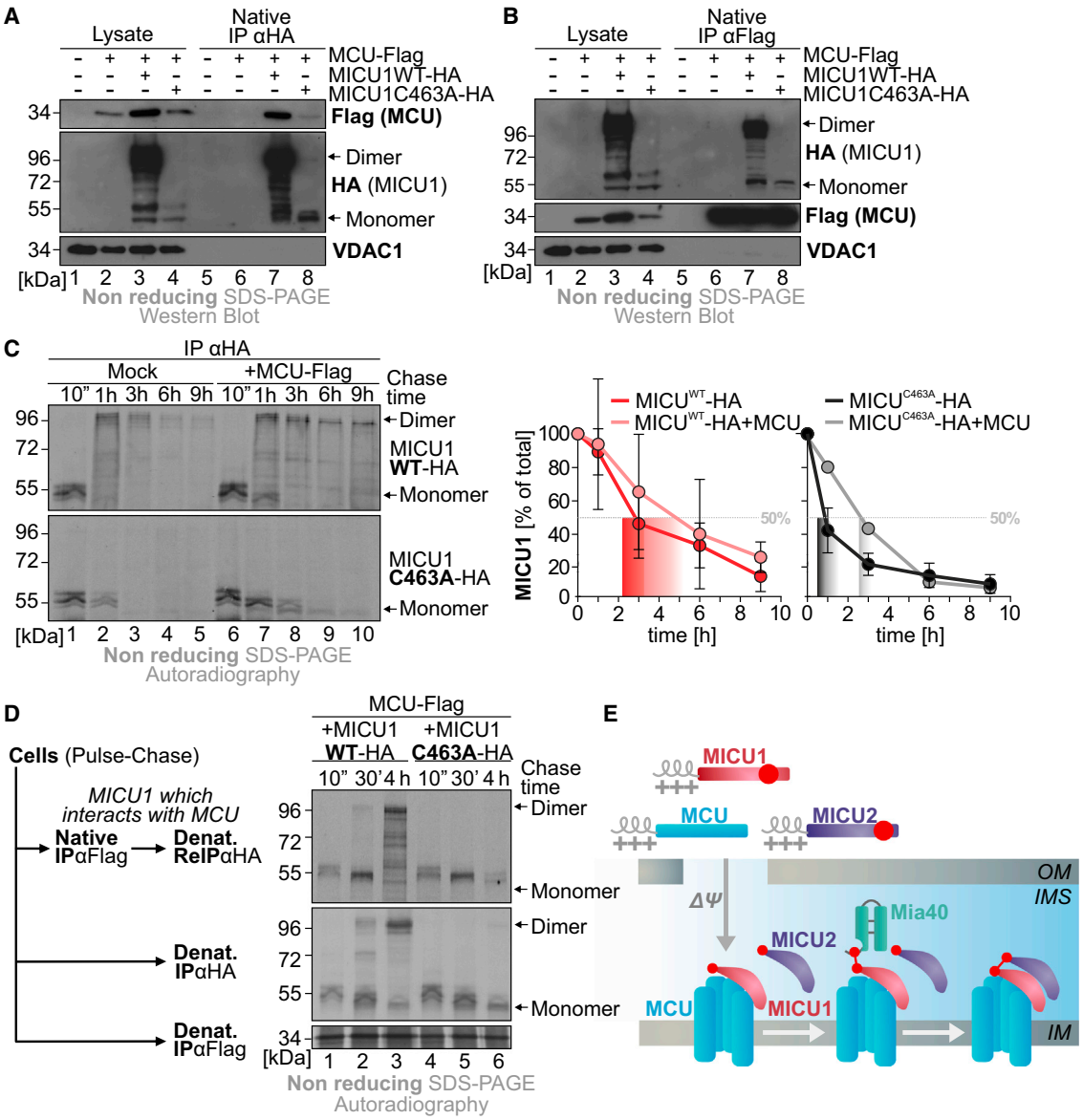

Figure 4. Disulfide Bond-Dependent Dimerization of MICU1 and MICU2 Takes Place on MCU

(A) MCU coprecipitates with both MICU1^{WT} and MICU1^{C463A}. Cells harboring an empty vector and cells expressing MCU-FLAG and in addition either an empty vector (Mock), MICU1^{WT}-HA, or MICU1^{C463A}-HA were lysed under mild native conditions. IP was performed against HA. Eluates were analyzed by immunoblotting against FLAG, HA, and VDAC1.

(B) Monomeric and dimeric MICU1^{WT} and MICU1^{C463A} coprecipitate with MCU. Cells harboring an empty vector and cells expressing MCU-FLAG and, in addition, either an empty vector (Mock), MICU1^{WT}-HA, or MICU1^{C463A}-HA were lysed under mild native conditions. IP was performed against FLAG. Eluates were analyzed by immunoblotting against FLAG, HA, and VDAC1.

(C) MICU1^{C463A}-HA is stabilized by coexpression of MCU-FLAG. Experiment was performed as described in Figure 3A except that cell lines expressing MICU1^{WT}-HA, MICU1^{C463A}-HA, MICU1^{WT}-HA/MCU-FLAG, or MICU1^{C463A}-HA/MCU-FLAG were used. IP was performed against HA. Eluates were analyzed by non-reducing SDS-PAGE and autoradiography. For quantification, the intensities of the protein bands at different times were analyzed with ImageJ and the half time calculated from the decrease in signal. Error bars represent SD.

(D) MICU1^{WT}-HA becomes oxidized while it is interacting with MCU. Cells expressing MCU-FLAG and MICU1^{WT}-HA were pulse labeled for 10 min and chased with non-radioactive methionine for the indicated times. To enrich the MICU1 species that interact with MCU during maturation, native IP was performed against FLAG and a subsequent denaturing RelP against HA. As control, direct IPs against FLAG and against HA were performed. Eluates were analyzed by non-reducing SDS-PAGE and autoradiography.

(E) Model for uniplex maturation and MICU1 dimerization. After membrane-potential-dependent import, monomeric MICU1 assembles on MCU. It then forms a disulfide-linked intermediate with Mia40 that is resolved by the recruitment of MICU2 and subsequent heterodimerization. The spatial preorientation of MICU1 and MICU2 on MCU could explain how an oxidoreductase like Mia40, which lacks extensive protein-protein interaction surfaces, can introduce intermolecular disulfide bonds.

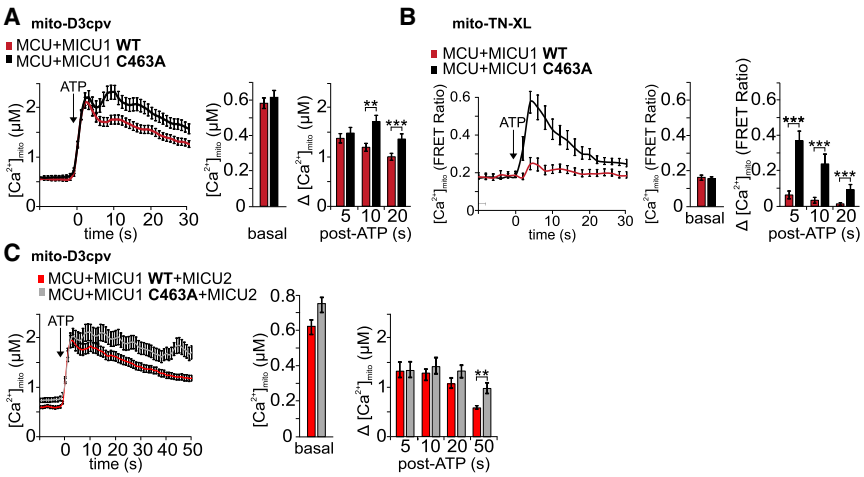

Figure 5. The Disulfide Bond in the MICU1-MCU2 Heterodimer Allows Regulation of MCU Activity

(A and B) Coexpression of MCU and MICU1^{C463A} increases mitochondrial Ca^{2+} uptake compared to coexpression of MCU and MICU1^{WT}. Ca^{2+} uptake was measured with D3cpv (A) and TN-XL (B), respectively. Left: ATP-induced mitochondrial Ca^{2+} uptake in HEK293 cells coexpressing MICU1^{WT} and MCU^{WT} (n = 160 for D3cpv, n = 10 for TN-XL) or MICU1^{C463A} and MCU^{WT} (n = 134 for D3cpv, n = 14 for TN-XL). Middle: Analysis of basal Ca^{2+} concentration in the mitochondrial matrix. Coexpression of MCU with MICU1^{WT} or MICU1^{C463A} does not result in increased $[Ca^{2+}]_{mito}$ levels before addition of ATP. Right: Analysis of mitochondrial Ca^{2+} uptake upon ATP treatment. Average $[Ca^{2+}]_{mito}$ values 5, 10, and 20 s after ATP addition. Coexpression of MCU and MICU1^{C463A} results in prolonged mitochondrial Ca^{2+} uptake. Error bars represent SEM.

(C) Coexpression of MCU and MICU1^{C463A} increases mitochondrial Ca^{2+} uptake even in the presence of MICU2. Left: ATP-induced mitochondrial Ca^{2+} uptake in HEK293 cells coexpressing MICU2, MCU and MICU1^{WT}, (n = 134 for D3cpv) or MICU1^{C463A} (n = 122 for D3cpv). Middle: Analysis of basal Ca^{2+} concentration in the mitochondrial matrix. Coexpression of MCU and MICU1^{WT} or MICU1^{C463A} does not result in increased $[Ca^{2+}]_{mito}$ levels before addition of ATP. Right: Analysis of mitochondrial Ca^{2+} uptake upon ATP treatment. Average $[Ca^{2+}]_{mito}$ values 5, 10, 20, and 50 s after ATP addition. Coexpression of MCU, MICU2, and MICU1^{C463A} results in prolonged mitochondrial Ca^{2+} uptake. Error bars represent SEM.

pathways in the IMS and thereby expand our knowledge on the function of Mia40.

MICU1 Represents the First Mia40 Substrate that Acquires an Intermolecular Disulfide Bond

MICU1 was the center of our study. Its localization had been intensely debated (Csordás et al., 2013; De Stefani et al., 2011; Hung et al., 2014; Mallilankaraman et al., 2012; Perocchi et al., 2010), and our study confirms the localization of MICU1 in the IMS by a complementary, independent approach. This also suggests that MICU1's EF hands sense IMS Ca^{2+} levels.

MICU1 differs from previously identified Mia40 substrates by several features: (1) it contains an MTS, which allows Mia40-independent import into mitochondria; (2) it plays a role in mitochondrial Ca^{2+} signaling (Csordás et al., 2013; de la Fuente et al., 2014; Mallilankaraman et al., 2012; Patron et al., 2014; Perocchi et al., 2010), a process that was not previously connected to the mitochondrial disulfide relay. This is also reflected by the decrease of Ca^{2+} uptake upon Mia40 depletion (Figures S5L–S5O), although it has to be emphasized that this might be a secondary effect, since Mia40 also imports, for example, components of the respiratory chain; (3) it is the first Mia40 substrate with an intermolecular disulfide bond. Heterodimerization with MICU2 is likely catalyzed by Mia40 as the redox-active cysteine 55 of Mia40 transiently interacts with cysteine 463 in MICU1, which at steady state, forms the mixed disufide bond with a cysteine residue of MICU2. Moreover, Mia40-MICU1 interaction preceded MICU1-MICU2 heterodimerization. Interestingly, we do not observe that stability or kinetics of disulfide bond formation are influenced by overexpression or siRNA-mediated depletion of Mia40 (Figure S3). This is in contrast to Mia40-dependent oxidation of classical Mia40 substrates for which mitochondrial import critically depends on oxidation and folding (Fischer et al., 2013). For these substrates, the rate of oxidative folding is limited by Mia40 levels, and consequently, lowered Mia40 levels impair import and oxidation, while increased Mia40 levels accelerate oxidative folding (Fischer et al., 2013). In contrast, we propose that in the case of MICU1, which becomes imported in a Mia40-independent manner, its initial binding to MCU and the recruitment of MICU2 to this complex, rather than the availability of Mia40, constitutes the time-critical step for intermolecular disulfide bond formation. We also think that binding to MCU allows the spatial alignment of MICU1 and MICU2 and that this enables intermolecular disulfide formation by the small oxidoreductase Mia40.

Ca^{2+}-Dependent Changes in Uniplex Composition Regulate Its Activity

Mutation of cysteine residue 463 did not prevent the interaction of MICU1 with MCU. However, it considerably decreased the stability of MICU1, which could be partially rescued by coexpression of MCU. MCU has a far longer half-life compared to MICU1 (Figure S4). This finding suggests that the mitochondrial uniplex is a dynamic entity in which MICU molecules can be exchanged without affecting MCU stability. This might in different tissues enable adaptation of the properties of the uniplex as, for example, MICU1-MICU2 heterodimers are replaced by MICU1-MICU1 or MICU1-MICU3 dimers. In line with this notion is our finding that changes in Ca^{2+} levels affected the interaction of MICU1 and MICU2 with MCU. It is tempting to interpret these results in the light of a recent report and our own data (Figure S5I) (Patron et al., 2014) that suggest an inhibitory role of MICU2 on the uniplex at resting Ca^{2+} concentrations. Release of the MICU1-MICU2 dimer from MCU upon increase in Ca^{2+} levels would remove this inhibitory unit from the uniplex, allowing rapid Ca^{2+} uptake. Decrease in Ca^{2+} levels would then lead to the re-recruitment of the MICU1-MICU2 heterodimer to MCU and a fast closure of the pore. It is tempting to hypothesize that the re-recruitment depends on EMRE, which might act as an anchor for the MICU heterodimer. In this scenario, EMRE could hold MICU in proximity to MCU at

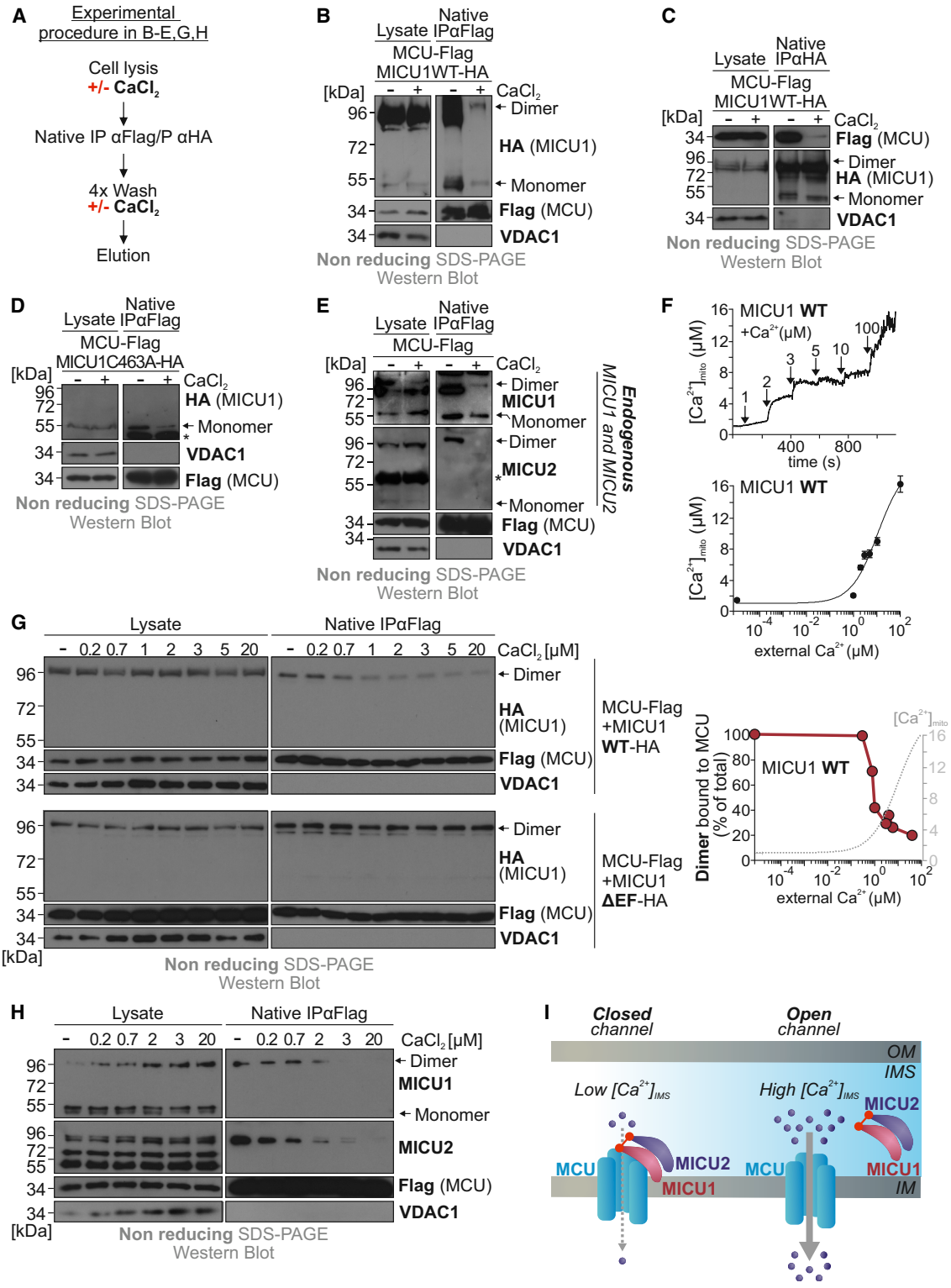

Figure 6. Ca^{2+} Modulates the Protein Composition of the Uniplex

(A) Experimental procedure used in the experiments shown in (B)–(E), (G), and (H). Mild cell lysis with 0.2% DDM as performed in the presence of Ca^{2+} or EGTA (- Ca^{2+}; for concentrations, see legends). Subsequently, MCU or MICU1 were enriched by IP. After washing and elution, samples were analyzed by immunoblotting. (B) MICU1-HA does not coprecipitate with MCU-FLAG in the presence of Ca^{2+}. The experiment was performed as described in (A). The mild lysis buffer either contained 5 mM Ca^{2+} or 5 mM EGTA. Eluates were analyzed by immunoblotting against FLAG, HA, and VDAC1.

(legend continued on next page)

high Ca^{2+} concentrations when the MICU dimer loses contact to MCU. It will be exciting to explore such a role for EMRE in the future.

EXPERIMENTAL PROCEDURES

Constructs, Cell Lines, siRNAs, and Antibodies

Refer to Tables S4 and S5, respectively. Antibodies: anti-HA (Sigma and Roche), anti-FLAG (Sigma), anti-Strep (iba-lifesciences), anti-MICU1 (Sigma), anti-MICU2 (Thermo Scientific), anti-Smac (Sigma), anti-Mitofilin (Proteintech), anti-LDH (Santa Cruz Biotechnology), and anti-Mia40 (self-made; Fischer et al., 2013). Secondary antibodies were directed against mouse or rabbit (BioRad). The following siRNAs were used: Hs_CHCHD4_5, Hs_CHCHD4_6, Hs_CBARA1_8, Hs_ CBARA1_12, Hs_EFHA1_7, and control siRNA (Quiagen).

Pulse-Chase Biogenesis Assay

These experiments were performed as previously described (Fischer et al., 2013). In short, cells were starved with cysteine and methionine-free medium (Sigma) for 15 min at 37°C and were pulse labeled for 10 min at 37°C with medium containing [35S]-methionine at a concentration of 200 μCi/ml (Perkin Elmer). Pulse labeling was stopped by adding chase medium containing 20 mM methionine. Importantly, care was taken to prevent post-lysis thiol-disulfide exchange reactions by incubation with 20 mM NEM before lysis.

For denaturing IPs, the chase was stopped after variable times at 37°C by adding PBS containing 20 mM NEM. Cells were centrifuged for 10 min at 500 × *g* and lysed in 250 μl 30 mM Tris [pH 8.1], 150 mM NaCl, 1 mM EDTA, and 1.6% SDS and boiled for 20 min. Then, 750 μl Triton X-100 was added, and the lysate was incubated for 1 hr at 4°C. Samples were cleared by centrifugation at 25,000 × *g* for 1 hr, and the supernatant was subjected to IP with antibodies conjugated to protein A beads at 4°C overnight. Beads were washed three times using lysis buffer containing Triton X-100 and once with lysis buffer without Triton X-100 and SDS. Proteins were eluted by adding Laemmli buffer (2% SDS, 60 mM Tris, pH 6.8, 10% glycerol and 0.0025% bromophenol blue) to the dried beads and subsequent boiling for 5 min at 95°C. Samples were analyzed by SDS-PAGE and autoradiography.

For native mild IPs, the chase was stopped after variable times at 37°C by adding native mild lysis buffer (50 mM HEPES [pH 7.4], 150 mM NaCl, 0.2% n-Dodecyl β-D-Maltopyranoside (DDM), and 5 mM EDTA). Cells were incubated for 10 min at 4°C and centrifuged for 1 hr at 25,000 × *g*. The supernatant was subjected to IP with antibodies conjugated to protein A beads at 4°C overnight. Samples were washed three times using native mild lysis buffer and once with lysis buffer without DDM. Elution and subsequent analysis was performed as described above.

Native Mild IP for Ca^{2+} Titration

Plates were washed with PBS and lysed while attached to the plate with native mild lysis buffer. The lysis buffer without Ca^{2+} contained 50 mM HEPES (pH 7.4), 150 mM NaCl, 0.2% n-Dodecyl β-D-Maltopyranoside (DDM), and 5 mM EDTA. To obtain the mild native lysis buffers with different concentrations of Ca^{2+} we mixed the mild native lysis buffer without Ca^{2+} with mild native lysis buffer with Ca^{2+} (50 mM HEPES [pH 7.4], 150 mM NaCl, 0.2% n- DDM, and 5 mM $CaCl_2$) according to http://maxchelator.stanford.edu/CaEGTA-TS.htm. Cells were lysed for 10 min at 4°C and centrifuged for 1 hr at 25,000 × *g*. The supernatant was subjected to IP with antibodies conjugated to protein A beads at 4°C overnight. Samples were washed three times using native mild lysis buffer and once with lysis buffer without DDM. Elution and subsequent analysis was performed as described above.

Stable Isotope Labeling in Cell Culture and Mass Spectrometry Analysis

Experiments were performed as described (Küttner et al., 2013). Affinity purifications with Strep-tactin beads were performed after NEM treatment of intact cells. For details, see the Supplemental Information.

Measurements of Mitochondrial Ca^{2+} Levels

Mitochondrial Ca^{2+} levels were measured using mitochondrial matrix-targeted genetically encoded Ca^{2+} sensors. Mitochondrial Ca^{2+} uptake in HEK293 cells was induced by 10 μM ATP and in HeLa cells by 100 μM histamine. Statistical significance was determined using two-sided unpaired Student's t test. For details see the Supplemental Information.

SUPPLEMENTAL INFORMATION

Supplemental Information includes six figures, five tables, and Supplemental Experimental Procedures and can be found with this article online at http://dx.doi.org/10.1016/j.cmet.2015.08.019.

AUTHOR CONTRIBUTIONS

J.R. and C.P. designed the study. Ca^{2+} experiments were designed by K.M.Z. and I.B. C.P., K.M.Z., V.K., and M.F. performed the experiments. All authors analyzed the data. J.R. and C.P. wrote the manuscript with help from I.B. and J.D.

ACKNOWLEDGMENTS

We thank Johannes Herrmann and Markus Hoth for constant support and Johannes Herrmann for critical comments on the manuscript. We thank Christian Junker for technical support. Work in the laboratories of J.R. (Rl2150/1-1 and

(C) MCU-FLAG does not coprecipitate with MICU1-HA in the presence of Ca^{2+}. The experiment was performed as in (B), except that MICU1-HA was immunoprecipitated. Eluates were analyzed by immunoblotting against FLAG, HA, and VDAC1.
(D) $MICU1^{C463A}$-HA binds in Ca^{2+}-sensitive manner to MCU-FLAG. The experiment was performed as in (B). Eluates were analyzed by immunoblotting against FLAG, HA, and VDAC1.
(E) Endogenous MICU1 and MICU2 do not coprecipitate with MCU-FLAG in the presence of Ca^{2+}. The experiment was performed as described in (B) except that a cell line that only expressed MCU-FLAG was used. Eluates were analyzed by immunoblotting against FLAG, MICU1, MICU2, and VDAC1. Asterisk: background band.
(F) Ca^{2+} uptake in mitochondria of semipermeabilized HEK293 cells. HEK293 cells stably expressing MCU-FLAG, $MICU1^{WT}$-HA were transfected with MICU2-Flag and 4mtD3cpv and were semi-permeabilized with 50 μM digitonin. Subsequently, the indicated amounts of Ca^{2+} were added and Ca^{2+} accumulation in mitochondria was quantified. Error bars represent SEM.
(G) Ca^{2+}-dependent binding of MICU1 to MCU is dependent on the EF hands in MICU1 and correlates with mitochondrial Ca^{2+} uptake activity. Analysis of MCU-FLAG -bound MICU1-HA in dependence of the Ca^{2+} concentration was performed as in (B), except that different Ca^{2+} concentrations were titrated and cell lines expressing MCU-Flag and either $MICU1^{WT}$-HA or $MICU1^{\Delta EF}$-HA were used. Eluates were analyzed by immunoblotting against FLAG, HA, and VDAC1. Quantification of bands was performed with ImageJ and correlated to the activity of mitochondrial Ca^{2+} uptake (from [F]).
(H) MICU1 and MICU2 binding to MCU exhibits similar Ca^{2+} concentration dependency. The experiment was performed as described in (G) except that a cell line which only expressed MCU-FLAG was used. Eluates were analyzed by immunoblotting against FLAG, MICU1, MICU2, and VDAC1.
(I) Model for Ca^{2+}-dependent rearrangement of the mitochondrial uniplex. At low local Ca^{2+} concentrations, MICU1-MICU2 heterodimers bind to MCU. Upon increase of Ca^{2+} concentrations in the IMS, Ca^{2+} binding to the EF hands in the MCIU1-MICU2 dimer leads to structural changes that lower the affinity toward MCU and lead to the release of MICU1-MICU2 from the uniplex.

1-2), I.B. (SFB1027 project C4, DFG grant BO3643/3-1 and HOMFORexcellent), and J.D. is funded by the Deutsche Forschungsgemeinschaft. C.P. was recipient of a Boehringer Ingelheim Fonds.

The authors declare no conflict of interest.

Received: December 10, 2014
Revised: May 24, 2015
Accepted: August 14, 2015
Published: September 17, 2015

REFERENCES

Banci, L., Bertini, I., Cefaro, C., Ciofi-Baffoni, S., Gallo, A., Martinelli, M., Sideris, D.P., Katrakili, N., and Tokatlidis, K. (2009). MIA40 is an oxidoreductase that catalyzes oxidative protein folding in mitochondria. Nat. Struct. Mol. Biol. *16*, 198–206.

Banci, L., Bertini, I., Calderone, V., Cefaro, C., Ciofi-Baffoni, S., Gallo, A., Kallergi, E., Lionaki, E., Pozidis, C., and Tokatlidis, K. (2011). Molecular recognition and substrate mimicry drive the electron-transfer process between MIA40 and ALR. Proc. Natl. Acad. Sci. USA *108*, 4811–4816.

Baughman, J.M., Perocchi, F., Girgis, H.S., Plovanich, M., Belcher-Timme, C.A., Sancak, Y., Bao, X.R., Strittmatter, L., Goldberger, O., Bogorad, R.L., et al. (2011). Integrative genomics identifies MCU as an essential component of the mitochondrial calcium uniporter. Nature *476*, 341–345.

Bien, M., Longen, S., Wagener, N., Chwalla, I., Herrmann, J.M., and Riemer, J. (2010). Mitochondrial disulfide bond formation is driven by intersubunit electron transfer in Erv1 and proofread by glutathione. Mol. Cell *37*, 516–528.

Chacinska, A., Koehler, C.M., Milenkovic, D., Lithgow, T., and Pfanner, N. (2009). Importing mitochondrial proteins: machineries and mechanisms. Cell *138*, 628–644.

Chaudhuri, D., Sancak, Y., Mootha, V.K., and Clapham, D.E. (2013). MCU encodes the pore conducting mitochondrial calcium currents. eLife *2*, e00704.

Csordás, G., Golenár, T., Seifert, E.L., Kamer, K.J., Sancak, Y., Perocchi, F., Moffat, C., Weaver, D., de la Fuente Perez, S., Bogorad, R., et al. (2013). MICU1 controls both the threshold and cooperative activation of the mitochondrial Ca^{2+} uniporter. Cell Metab. *17*, 976–987.

de la Fuente, S., Matesanz-Isabel, J., Fonteriz, R.I., Montero, M., and Alvarez, J. (2014). Dynamics of mitochondrial Ca2+ uptake in MICU1-knockdown cells. Biochem. J. *458*, 33–40.

De Stefani, D., Raffaello, A., Teardo, E., Szabò, I., and Rizzuto, R. (2011). A forty-kilodalton protein of the inner membrane is the mitochondrial calcium uniporter. Nature *476*, 336–340.

Fischer, M., Horn, S., Belkacemi, A., Kojer, K., Petrungaro, C., Habich, M., Ali, M., Küttner, V., Bien, M., Kauff, F., et al. (2013). Protein import and oxidative folding in the mitochondrial intermembrane space of intact mammalian cells. Mol. Biol. Cell *24*, 2160–2170.

Gabriel, K., Milenkovic, D., Chacinska, A., Müller, J., Guiard, B., Pfanner, N., and Meisinger, C. (2007). Novel mitochondrial intermembrane space proteins as substrates of the MIA import pathway. J. Mol. Biol. *365*, 612–620.

Gross, D.P., Burgard, C.A., Reddehase, S., Leitch, J.M., Culotta, V.C., and Hell, K. (2011). Mitochondrial Ccs1 contains a structural disulfide bond crucial for the import of this unconventional substrate by the disulfide relay system. Mol. Biol. Cell *22*, 3758–3767.

Hajnóczky, G., Davies, E., and Madesh, M. (2003). Calcium signaling and apoptosis. Biochem. Biophys. Res. Commun. *304*, 445–454.

Hangen, E., Féraud, O., Lachkar, S., Mou, H., Doti, N., Fimia, G.M., Lam, N.V., Zhu, C., Godin, I., Muller, K., et al. (2015). Interaction between AIF and CHCHD4 Regulates Respiratory Chain Biogenesis. Mol. Cell *58*, 1001–1014.

Herrmann, J.M., and Riemer, J. (2010). The intermembrane space of mitochondria. Antioxid. Redox Signal. *13*, 1341–1358.

Hung, V., Zou, P., Rhee, H.W., Udeshi, N.D., Cracan, V., Svinkina, T., Carr, S.A., Mootha, V.K., and Ting, A.Y. (2014). Proteomic mapping of the human mitochondrial intermembrane space in live cells via ratiometric APEX tagging. Mol. Cell *55*, 332–341.

Kamer, K.J., and Mootha, V.K. (2014). MICU1 and MICU2 play nonredundant roles in the regulation of the mitochondrial calcium uniporter. EMBO Rep. *15*, 299–307.

Kawano, S., Yamano, K., Naoé, M., Momose, T., Terao, K., Nishikawa, S., Watanabe, N., and Endo, T. (2009). Structural basis of yeast Tim40/Mia40 as an oxidative translocator in the mitochondrial intermembrane space. Proc. Natl. Acad. Sci. USA *106*, 14403–14407.

Klöppel, C., Suzuki, Y., Kojer, K., Petrungaro, C., Longen, S., Fiedler, S., Keller, S., and Riemer, J. (2011). Mia40-dependent oxidation of cysteines in domain I of Ccs1 controls its distribution between mitochondria and the cytosol. Mol. Biol. Cell *22*, 3749–3757.

Koch, J.R., and Schmid, F.X. (2014). Mia40 targets cysteines in a hydrophobic environment to direct oxidative protein folding in the mitochondria. Nat. Commun. *5*, 3041.

Kojer, K., Bien, M., Gangel, H., Morgan, B., Dick, T.P., and Riemer, J. (2012). Glutathione redox potential in the mitochondrial intermembrane space is linked to the cytosol and impacts the Mia40 redox state. EMBO J. *31*, 3169–3182.

Küttner, V., Mack, C., Rigbolt, K.T., Kern, J.S., Schilling, O., Busch, H., Bruckner-Tuderman, L., and Dengjel, J. (2013). Global remodelling of cellular microenvironment due to loss of collagen VII. Mol. Syst. Biol. *9*, 657.

Lionaki, E., Aivaliotis, M., Pozidis, C., and Tokatlidis, K. (2010). The N-terminal shuttle domain of Erv1 determines the affinity for Mia40 and mediates electron transfer to the catalytic Erv1 core in yeast mitochondria. Antioxid. Redox Signal. *13*, 1327–1339.

Longen, S., Bien, M., Bihlmaier, K., Kloeppel, C., Kauff, F., Hammermeister, M., Westermann, B., Herrmann, J.M., and Riemer, J. (2009). Systematic analysis of the twin cx(9)c protein family. J. Mol. Biol. *393*, 356–368.

Mallilankaraman, K., Doonan, P., Cárdenas, C., Chandramoorthy, H.C., Müller, M., Miller, R., Hoffman, N.E., Gandhirajan, R.K., Molgó, J., Birnbaum, M.J., et al. (2012). MICU1 is an essential gatekeeper for MCU-mediated mitochondrial Ca(2+) uptake that regulates cell survival. Cell *151*, 630–644.

Milenkovic, D., Ramming, T., Müller, J.M., Wenz, L.S., Gebert, N., Schulze-Specking, A., Stojanovski, D., Rospert, S., and Chacinska, A. (2009). Identification of the signal directing Tim9 and Tim10 into the intermembrane space of mitochondria. Mol. Biol. Cell *20*, 2530–2539.

Patron, M., Checchetto, V., Raffaello, A., Teardo, E., Vecellio Reane, D., Mantoan, M., Granatiero, V., Szabò, I., De Stefani, D., and Rizzuto, R. (2014). MICU1 and MICU2 finely tune the mitochondrial Ca2+ uniporter by exerting opposite effects on MCU activity. Mol. Cell *53*, 726–737.

Perocchi, F., Gohil, V.M., Girgis, H.S., Bao, X.R., McCombs, J.E., Palmer, A.E., and Mootha, V.K. (2010). MICU1 encodes a mitochondrial EF hand protein required for Ca(2+) uptake. Nature *467*, 291–296.

Plovanich, M., Bogorad, R.L., Sancak, Y., Kamer, K.J., Strittmatter, L., Li, A.A., Girgis, H.S., Kuchimanchi, S., De Groot, J., Speciner, L., et al. (2013). MICU2, a paralog of MICU1, resides within the mitochondrial uniporter complex to regulate calcium handling. PLoS ONE *8*, e55785.

Raffaello, A., De Stefani, D., Sabbadin, D., Teardo, E., Merli, G., Picard, A., Checchetto, V., Moro, S., Szabò, I., and Rizzuto, R. (2013). The mitochondrial calcium uniporter is a multimer that can include a dominant-negative pore-forming subunit. EMBO J. *32*, 2362–2376.

Rizzuto, R., De Stefani, D., Raffaello, A., and Mammucari, C. (2012). Mitochondria as sensors and regulators of calcium signalling. Nat. Rev. Mol. Cell Biol. *13*, 566–578.

Sancak, Y., Markhard, A.L., Kitami, T., Kovács-Bogdán, E., Kamer, K.J., Udeshi, N.D., Carr, S.A., Chaudhuri, D., Clapham, D.E., Li, A.A., et al. (2013). EMRE is an essential component of the mitochondrial calcium uniporter complex. Science *342*, 1379–1382.

Sideris, D.P., Petrakis, N., Katrakili, N., Mikropoulou, D., Gallo, A., Ciofi-Baffoni, S., Banci, L., Bertini, I., and Tokatlidis, K. (2009). A novel intermembrane space-targeting signal docks cysteines onto Mia40 during mitochondrial oxidative folding. J. Cell Biol. *187*, 1007–1022.

Terziyska, N., Grumbt, B., Kozany, C., and Hell, K. (2009). Structural and functional roles of the conserved cysteine residues of the redox-regulated import

receptor Mia40 in the intermembrane space of mitochondria. J. Biol. Chem. *284*, 1353–1363.

Vögtle, F.N., Burkhart, J.M., Rao, S., Gerbeth, C., Hinrichs, J., Martinou, J.C., Chacinska, A., Sickmann, A., Zahedi, R.P., and Meisinger, C. (2012). Intermembrane space proteome of yeast mitochondria. Mol. Cell. Proteomics *11*, 1840–1852.

Weckbecker, D., Longen, S., Riemer, J., and Herrmann, J.M. (2012). Atp23 biogenesis reveals a chaperone-like folding activity of Mia40 in the IMS of mitochondria. EMBO J. *31*, 4348–4358.

Wrobel, L., Trojanowska, A., Sztolsztener, M.E., and Chacinska, A. (2013). Mitochondrial protein import: Mia40 facilitates Tim22 translocation into the inner membrane of mitochondria. Mol. Biol. Cell *24*, 543–554.